JOURNAL OF MATERIALS SCIENCE 30 (1995) 5399–5404

Processing and microstructure of porous and dense PZT thick films on Al_2O_3

J. F. FERNANDEZ, E. NIETO, C. MOURE, P. DURAN
Electroceramics Department, Instituto de Ceramica y Vidrio, CSIC, 28500 Arganda del Rey, Madrid, Spain

R. E. NEWNHAM
Materials Research Laboratory, Pennsylvania State University, University Park, PA 16802, USA

The processing of porous PZT thick-film ceramics on Al_2O_3 has been studied. The films were screen-printed from a thixotropic ink of PZT with a 58% solids content. The thick films were sintered between 1000 and 1150 °C for 2 h. The sintered films show a 10 μm thickness and an average pore diameter ranging from 1–2 μm. The PZT forms a continuous skeleton that can be filled with the desired polymer. Dense and continuous PZT films were fabricated by screen-printing PZT ink on previously electroded Al_2O_3 substrates with Ag/Pd 70/30 paste. Densification of the PZT was obtained by sintering near the liquidus temperature of the Ag–Pd system.

1. Introduction

PZT/polymer composites and porous PZT ceramics have been extensively investigated since Newnham *et al.* [1] first reported the importance of connectivity in piezoelectric composites. The fabrication of piezoelectric composites requires careful replacement of a portion of the piezoelectric ceramic with a polymer. This replacement allows the reduction of the acoustic impedance of the piezoelectric ceramics for underwater sonar or biomedical systems. In recent years, research efforts in this field have been directed towards material fabrication techniques, finite element modelling, and the use of electrostrictive ceramics.

In 3–3 composites, each of the constituent phases is continuously self-connected in three dimensions to give two interlocking skeletons in intimate contact with one another. Skinner *et al.* [2] prepared 3–3 type composite materials consisting of porous PZT ceramics with coral skeleton structures, duplicated by the "replamine form" process, into which silicone rubber was injected. Shrout *et al.* [3] developed a more readily produced type of porous ceramics using burned-out plastic spheres and PZT powder in an organic binder. When carefully sintered, a porous PZT skeleton was formed, which was later backfilled with polymers to form a 3–3 composite. Hayashi *et al.* [4] investigated the processing of porous 3–3 type PZT ceramics with controlled porosity by using capsule-free O_2-HIP (hot isostatic pressing). This method allows little densification of porous PZT bodies during sintering, resulting in an increase of the contact area between PZT particles but without changing the pore volume and distribution. The HIPed porous ceramic possessed a large permittivity and small despolarizing factor of about half that of normally sintered porous PZT bodies. Waller *et al.* [5] used a replication process to fabricate woven PZT/polymer matrix composites with finely spaced structures. This process involves using a carbon fibre material which determines the form of the PZT ceramic phase.

Many of the piezocomposites reported in the literature show interconnected porosity with pore size ranging from 50–600 μm [2–4]. In calcium-modified $PbTiO_3$ ceramics of similar porosity, the smaller pore size samples had better properties than those with large pore size [6]. In these materials, the increase in dielectric properties with increasing porosity was related to superior pore-interconnectivity which promoted stress transfer to the skeleton more effectively [6].

Porous ceramics are of interest for a variety of applications including sensors, bioceramics, and membranes. This study focuses on the processing of porous 3–3 type PZT thick-film ceramics with controlled porosity. The porous ceramics were fabricated on Al_2O_3 substrates. Dense PZT thick films can be sintered by using an electrode interlayer.

2. Experimental procedure

$Pb(Zr_{0.53}Ti_{0.47})O_3$ (PZT) ceramic powders were prepared following a modified conventional oxide process starting from analytical reagent grade oxides [7]. In this process, TiO_2 and ZrO_2 were placed in 1:1 ratio of isopropyl alcohol to water. Oxalic acid was added to the suspension. The suspension was heated and continuously stirred, and a stoichiometric

0022–2461

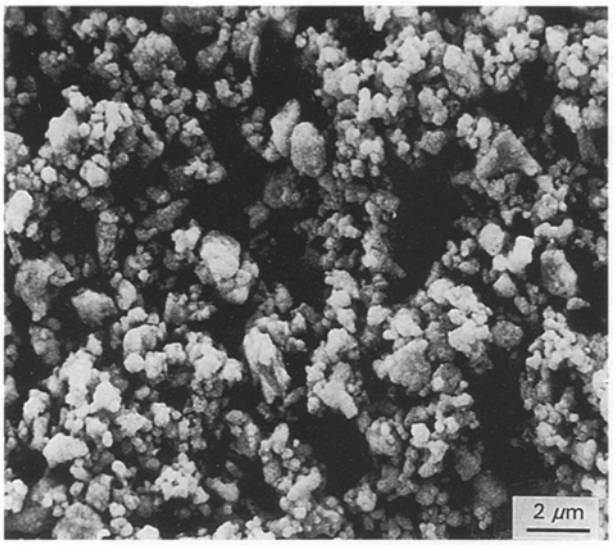

Figure 1 Scanning electron micrograph of synthesized powder of PZT.

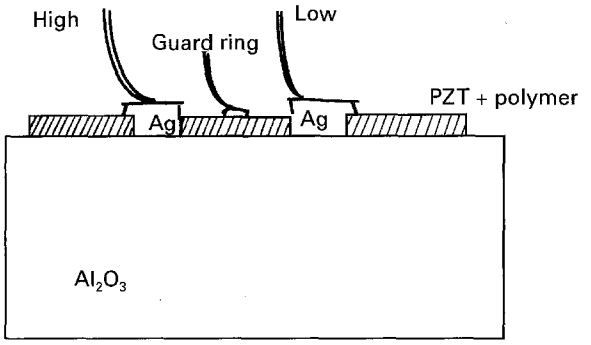

Figure 2 The geometry of the electrodes placed on porous PZT thick films filled with polymer.

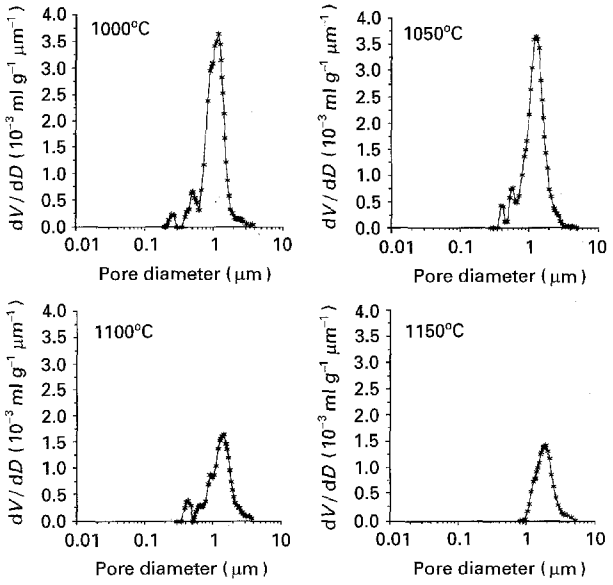

Figure 3 Porosity curves of the samples sintered at different temperatures.

amount of lead oxide was added. The dried powders were amorphous and were calcined at 700 °C for 4 h and attrition milled with zirconia balls. The thermal treatment crystallized the powders into a tetragonal perovskite phase plus zirconia and lead oxide that remained partially unreacted. The average particle size was 0.4 μm as measured by both XRD analysis and laser Coulter methods. A small portion of the particles were larger than 1.5 μm, corresponding to the small agglomerates observed by SEM analysis (Fig. 1).

PZT ink was prepared by ultrasonic dispersion of the ceramic powders [8] in α-terpineol and 2–2 (buthoxyethoxy) ethyl acetate. The as-prepared paste was milled with ethyl cellulose to give the thixotropic characteristic required of the inks used in screen-printing. The ink was screen-printed on 5.2×5.2 cm^2 99% Al_2O_3 substrates having a roughness of 0.3 μm (Rubalit 710, Hoescht). The substrates were laser pre-cut in order to obtain samples of 2.5×1 cm^2. A stainless steel 45° oriented 320 mesh screen was used. Some substrates were previously electroded with 70/30 Ag/Pd paste (6142D, Du Pont). The electrode was sintered at 850 °C in a typical electrode sintering cycle of 1 h. The screen-printed films were dried at 150 °C for 15 min, and the organic vehicle was burned-out at 500 °C. The samples were sintered in high-purity alumina crucibles at a heating rate of 3 °C min^{-1}, between 1000 and 1150 °C for 2 h. A lead-rich atmosphere was maintained by placing $PbZrO_3$ + 5 wt % ZrO_2 powders near the samples. The porosity distribution of the sintered thick films was evaluated with a mercury porosimeter (Autopore II 9220) with a mercury filling pressure from 4×10^{-3} MPa up to 400 MPa. In order to ensure that the stem volume used reached an adequate value, several samples were used each time. The microstructure of the as-sintered samples and transverse polished cross-section were examined by scanning electron microscopy (Zeiss DSM 950). Crystalline evolution was followed by X-ray diffraction (XRD, Siemens D-5000 Diffractometer).

The thick films sintered at 1100 °C for 2 h were filled with vinyl chloride acetate by dipping the porous films in boiling polymer. Silver epoxy electrodes were applied with syringe under an optical microscope on previously machined canals (Fig. 2). The distance between canals was 1 mm. Silver wires were bonded to the electrodes by using silver epoxy. A parallel electrode arrangement was developed in order to reach higher capacitance values. The dielectric constant was calculated from capacitance data measured on an HP 4192A impedance analyser at 1 kHz, 1 V.

3. Results and discussion

3.1. Porous PZT thick films

Fig. 3 shows the pore diameter distribution for selected sintering temperatures and Fig. 4 shows the microstructure of these sintered samples. The porosity of the alumina substrates in this range (< 10 μm) is negligible compared to the porosity of the sintered PZT thick films. The alumina substrates exhibited pore diameters ranging from 8–120 μm (not shown) that are attributed to the fracture surfaces of the laser pre-cut substrates. The pore-size curves show different contributions to the overall porosity volume. The porosity of the thick films ranges from 0.1–4 μm, which

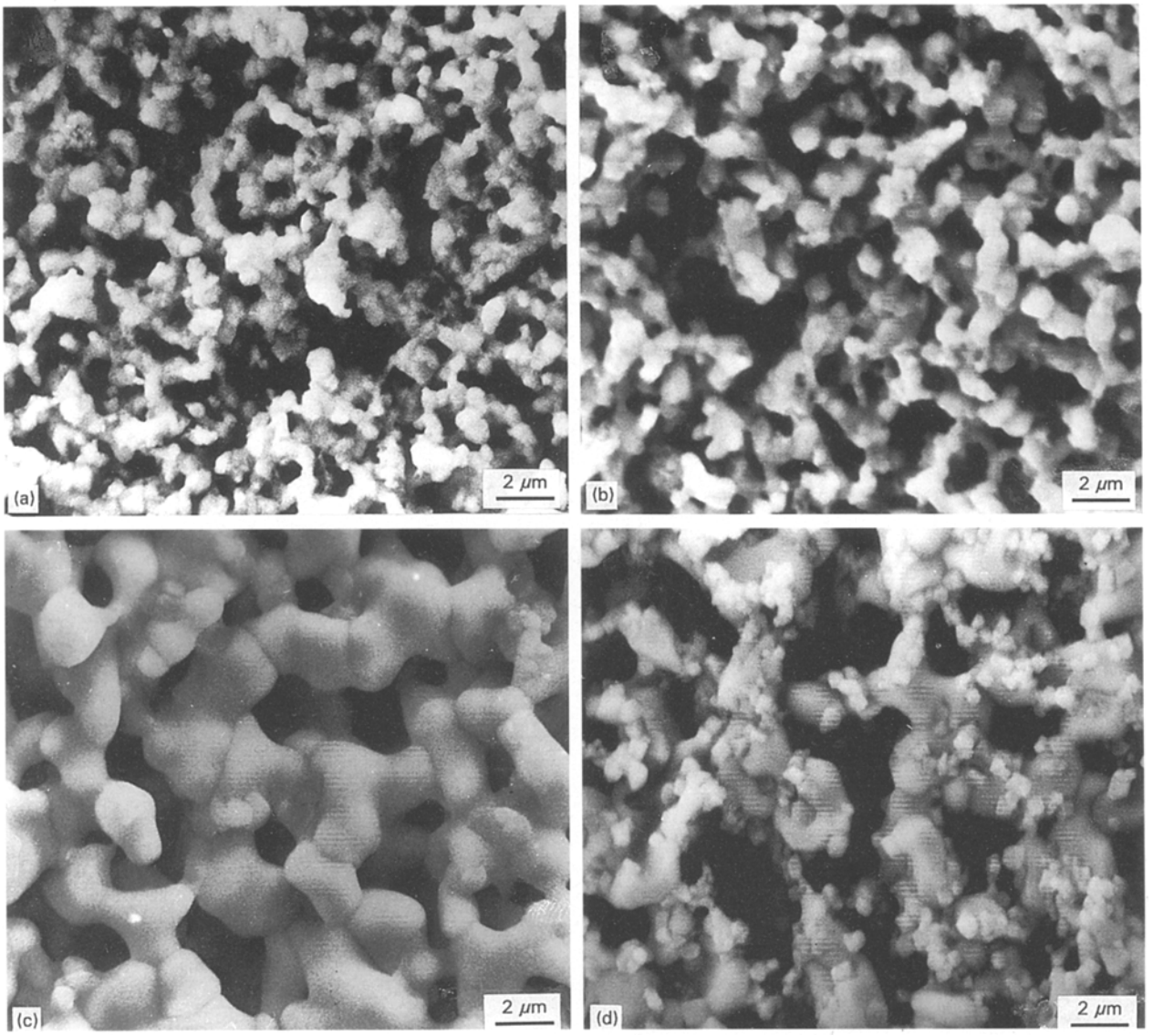

Figure 4 Scanning electron micrographs of samples sintered at (a) 1000 °C, 2 h; (b) 1050 °C, 2 h; (c) 1100 °C, 2 h; and (d) 1150 °C, 2 h.

can be attributed to interparticle porosity, or interaggregate porosity [9].

The microstructure of the samples sintered at 1000 and 1050 °C for 2 h shows a similar structure. The PZT particles form chains of grains. Small aggregates consisting of several grains and causing discontinuities in the skeleton ceramic structure can be found. The sample sintered at 1100 °C for 2 h gave an interconnected well-densified 3–3 ceramic/pore structure (Figs 4c and 5). The chain of grains sintered to form bigger grains that are connected almost grain to grain. A few small particles remained in aggregates or on the surface of the larger grains. The sample sintered at 1150 °C for 2 h shows a higher proportion of such small particles (Fig. 4d). These small particles have cubic or quasi-cubic shapes.

Fig. 6 shows the XRD patterns of thick films sintered at several temperatures. It was observed that the porous ceramic layer crystallizes as a perovskite phase. The XRD patterns also showed the Al_2O_3 substrate phase. For a sample sintered at 1050 °C for 2 h the XRD pattern shows a mixture of

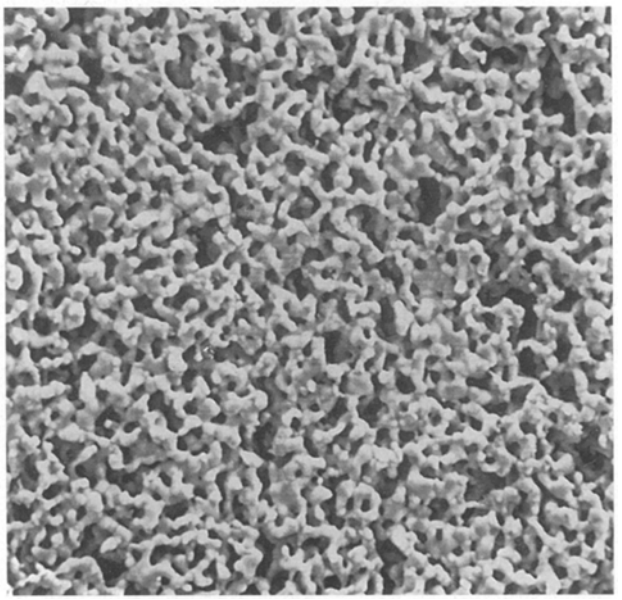

Figure 5 Scanning electron micrograph of PZT sample sintered at 1100 °C showing 3–3 connectivity.

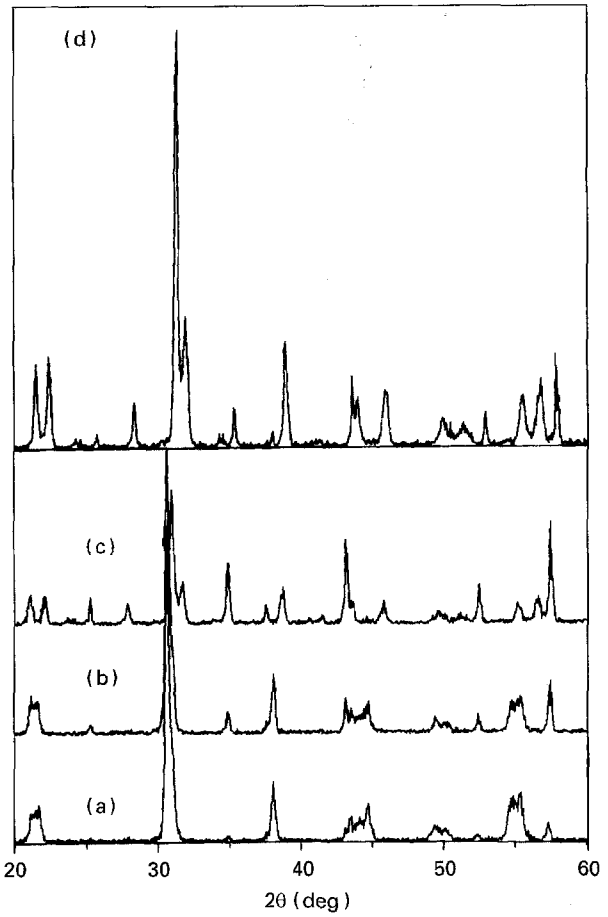

Figure 6 XRD pattern of samples sintered at (a) 1050 °C, 2 h; (b) 1100 °C, 2 h; (c) 1150 °C, 2 h (all with buffer); and (d) 1100 °C, 2 h (without buffer).

rhombohedral and tetragonal phases. The perovskite phase transforms to a pure tetragonal phase as the sintering temperature is raised. A sample sintered at 1150 °C for 2 h shows the presence of PbO as second phase and confirmed the crystalline nature of the small particles with cubic shape observed at the surface of the sintered PZT. PbO crystals can be attributed to both the PbO losses in the ceramic matrix that produce a shift in composition towards the $PbTiO_3$ region [10], accompanied by PbO crystallization from the lead-rich atmosphere generated by the buffer. In order to confirm these results, samples were sintered without PbO buffer in sealed crucibles. Fig. 6d shows the XRD pattern at 1100 °C for 2 h unbuffered sintered film. The presence of PbO is notorious at this temperature as in the highly sintered samples obtained with buffered systems. The higher surface area of the porous structures favours the PbO losses from the ceramic matrix, and as a consequence the displacement of the composition towards high $PbTiO_3$ region. Buffered atmospheres permit control of the PbO losses, but as the temperature increases, the higher activity of lead saturates the atmosphere and PbO crystals are nucleated as secondary crystalline phase at the surface of PZT particles.

Bulk ceramic samples from the same PZT powder were sintered in the same temperature range as the thick films, again in buffered arrangements. The tetragonality of the bulk ceramics showed a clear displacement towards the $PbTiO_3$-rich region for

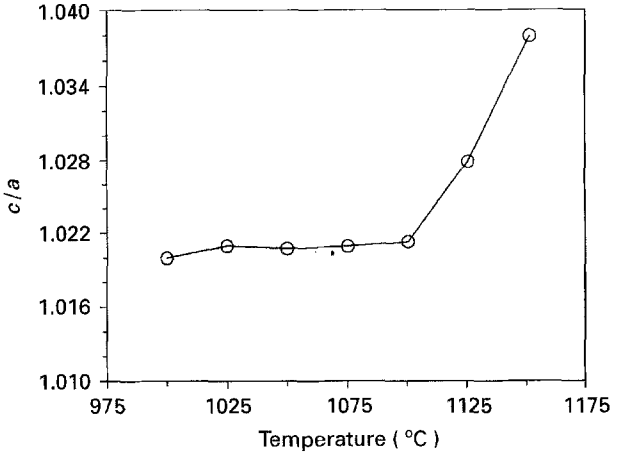

Figure 7 Tetragonality as a function of the sintering temperature in PZT bulk ceramics.

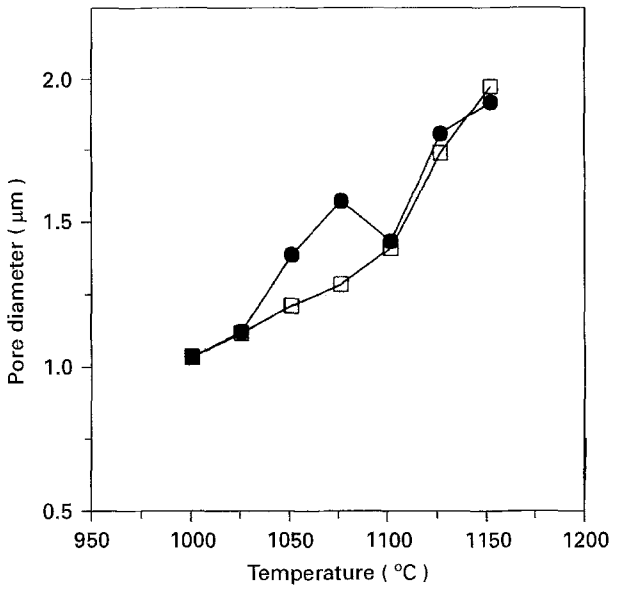

Figure 8 (□) Average pore size and (●) main pore size maximum for different sintering temperatures.

sintering temperatures above 1100 °C (Fig. 7), although zirconia phases could not be confirmed by XRD analysis in the ceramic matrix.

Taking into account the microstructure and the porosity curves, three different contributions to the porosity are proposed.

1. Low interparticle porosity: this type of porosity ranged below ~0.7 μm; its contribution to the overall porosity is very low and can be attributed to both the interparticle porosity of the aggregates and to the pores formed during the sintering of the small particles that are not completely eliminated.

2. Main interparticle porosity; this porosity type is the most important in terms of volume, and shows a narrow pore-size distribution that indicates a high degree of homogeneity.

3. High interparticle porosity: these pores are the tail above 2 μm that corresponds to the discontinuities in the ceramic skeleton structure (Fig. 5). These discontinuities are attributed to both the burn-out process and to the presence of organic agglomerates that were not completely eliminated during the ink preparation, mainly ethyl cellulose agglomerates.

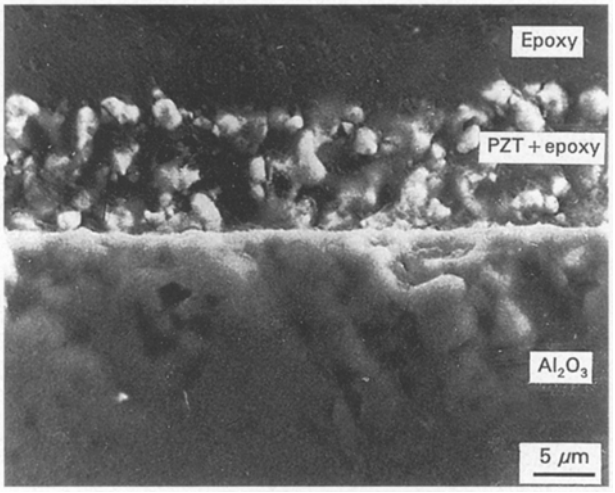

Figure 9 Scanning electron micrograph of a polished cross-section of PZT thick film sintered at 1100 °C, 2 h and filled with epoxy resins.

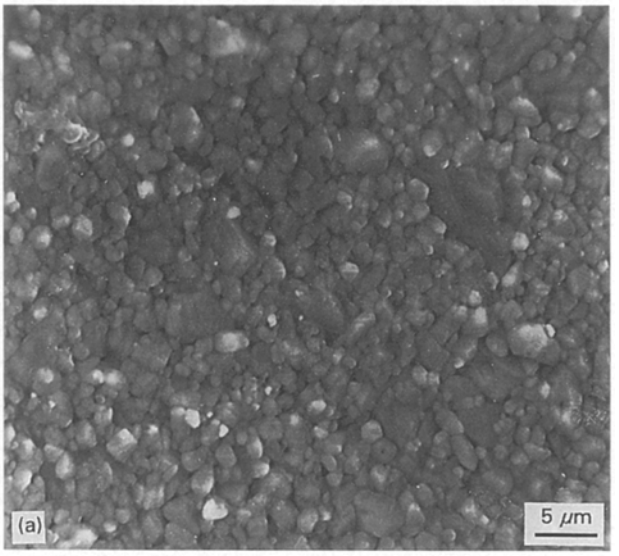

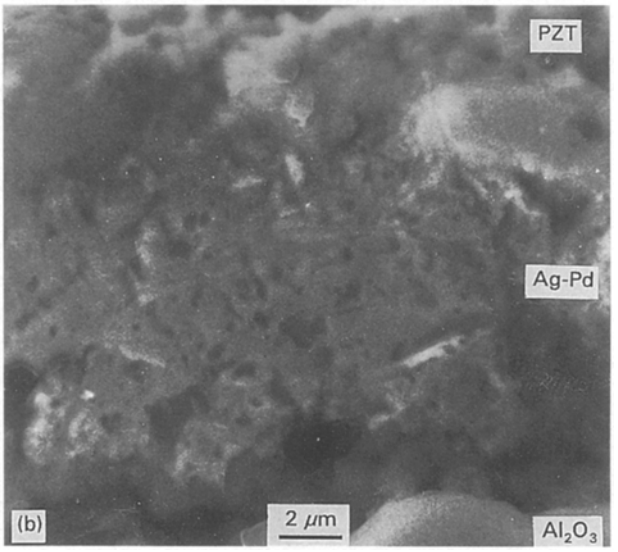

Figure 10 Scanning electron micrographs of dense PZT thick film sintered at 1100 °C, 2 h; (a) as-sintered surface and, (b) polished cross-section of the thick film.

The porosity decreased when grain growth took place. The sample sintered at 1100 °C for 2 h had an average area pore size of 1.42 μm (Fig. 8). The average pore size increases almost linearly with the sintering temperature up to 1075 °C, but the main pore size maximum increased more rapidly than the average pore size for lower temperatures; this can be attributed to the pore coalescence process. When grain growth takes place, the average pore size and the medium pore diameter are similar. The grain growth also favours the process of pore coalescence and the slope of the pore diameter as a function of the sintering temperature is approximately three times higher than the slope in the grain growth control temperature range. The pore-size distribution does not change significantly even when the particles lose their initial shape, and at this sintering stage the pore size does not increase. That means that the sintering of PZT takes place without significantly modifying the skeleton structure. The initial dispersion of the powders has a very important role in the sintering mechanism. The small particles that formed aggregates sintered together, resulting in larger particles. These new larger particles were surrounded by both particles and pores. The number of contact points between particles decreased and the probability of formation of new sintering necks decreased with increasing grain growth. As grain growth takes place the high interparticle porosity extends to even higher values, probably because of excessive shrinkage of the film. On the other hand, the appearance of PbO as second crystalline phase in the film nucleates on the surface of the perovskite particles when the elimination of the low interparticle porosity is complete. That fact, in conjunction with the grain growth process and the shrinkage of the films at higher temperatures, supports the hypothesis that the sintering at high temperatures is driven by the surface diffusion of Pb^{2+} cations, which also accelerates the evaporation of lead.

The as-sintered thick films show about a ~10 μm thickness and good 3–3 connectivity (Fig. 9). Epoxy resin adequately filled the porous structure to give good piezocomposites. Both the thickness and the excellent pore connectivity are the reasons for such behaviour.

The dielectric constant of the sample sintered at 1100 °C for 2 h and filled with polymer reached a value of 155. According to Wersing *et al.* [11], the effective permittivity, ε*, of two-phase composite bodies can be calculated from the following simplified equation

$$\varepsilon^*(p) = \varepsilon(1 - 3p/2) \quad (1)$$

where ε is the relative permittivity of the ceramic component. Assuming the dielectric constant of the bulk ceramic to be 1105, the calculated porosity of the thick film is ~58%. In this calculation the contribution of the polymer was neglected. From the porosity studies, the porosity volume fraction is estimated as only 44%. The higher porosity estimated from the dielectric data is probably associated with the high interparticle porosity and the presence of microcracking in the ceramic arising from thermal expansion

mismatch [12] during the polymer filling process. The low dielectric constant may also be attributed to Al^{3+} cation diffusion into the perovskite thick film during the sintering process. EDAX (not shown) analysis confirmed such diffusion, but the complexity of the sample does not allow quantification of the diffusion profile.

The dielectric breakdown of the sample sintered at 1100 °C for 2 h occurs at 24 kV cm^{-1}. Taking into account the estimated porosity of 58% from dielectric measurements, the equivalent ceramic breakdown is approximately 41 kV cm^{-1}. If the porosity is only 44%, the equivalent breakdown is 55 kV cm^{-1}, which is comparable to the value obtained in the bulk ceramic (> 65 kV cm^{-1}). This number provides a measure of the quality of the porous ceramic.

3.2. Dense PZT films

Fig. 10a shows the microstructure of dense PZT thick films. The microstructure is a duplex one with most of the porosity located at the triple point junctions. The big grains are typically faceted perovskite grains. The thickness of the film is ~ 5 μm (Fig. 10b). In this case the thickness reduction favours the elimination of the pores and the densification of the ceramic films. The driving forces for the sintering are assisted by the liquidus formed in the Ag/Pd system at this temperature. The Al_2O_3 substrate reacts slightly with the electrode to provide good adhesion for the film. In the dense PZT films the presence of Al^{3+} cations is avoided because of the inhibiting effect of the metallic interlayer [13]. Dielectric measurements were not carried out because of the presence of flaws that provoke electric shorts. Future works in this field might involve sequential screen printing of thick film layers as has been recently demonstrated [14, 15].

4. Conclusion

A method for processing porous and dense thick PZT films has been developed. The initial distribution of dispersed PZT particles in an organic medium leads to a skeleton structure with 3–3 pattern connectivity. The porous PZT thick films can easily be filled with polymer. By adjusting the process parameters a $1/2\lambda$ thickness (half wavelength of a desirable resonant frequency) [16] thick film piezocomposite can be fabricated. This method is easily adapted to curved surfaces and allows the piezoelectric transducer to be focused without additional treatment. This process could also serve as an integrating step between electroceramic materials and hybrid circuit technologies.

Acknowledgements

The authors thank the Spanish Science Ministry Commission for the financial support of this work (CICYT MAT-1386-E) and National Science Foundation under contract (DMR-MRG 9223847), Dr Rubio for porosimeter facilities and Professor J. L. Acosta for polymer filling.

References

1. R. E. NEWNHAM, D. P. SKINNER and L. E. CROSS, *Mater. Res. Bull.* **13** (1978) 525.
2. D. P. SKINNER, R. E. NEWNHAM and L. E. CROSS, *ibid.* **13** (1978) 599.
3. T. R. SHROUT, W. A. SCHULZE and J. V. BIGGERS, *ibid.* **14** (1979) 1553.
4. T. HAYASHI, S. SUGAHARA and K. OKAZAKI, *Jpn J. Appl. Phys.* **30** (9B) (1991) 2243.
5. D. J. WALLER, A. SAFARI and R. J. CARD, in "Proceedings of the IEEE International Symposium on Applications on Ferroelectrics 1990", edited by S. B. Krupanidhi and S. K. Kurtz (IEEE, Inc., Piscataway, NJ, 1991) pp. 82–5.
6. K. H. YOON and M. J. LEE, *Ferroelectrics* **119** (1991) 53.
7. E. NIETO, J. F. FERNANDEZ, C. MOURE and P. DURAN, *J. Mater Sci.* (1995) in press.
8. T. CHARTIER, E. JORGE and P. BOCH, *J. Phys.* **III** (1991) 689.
9. W. F. M. GROOT ZEVERT, A. J. A. WINNUBST, G. S. A. THEUNISSEN and A. J. BURGRAAF, *J. Mater. Sci.* **25** (1990) 3449.
10. S. K. SAHA, D. C. AGRAWAL, *Am. Ceram. Soc. Bull.* **71** (1992) 1424.
11. W. WERSING, K. LUBITZ and J. MOHAUPT, *Ferroelectrics* **68** (1986) 77.
12. T. OTA, J. TAKAHASHI and I. YAMAI, in "Electronic Ceramic Materials", edited by J. Nowotny (Trans. Tech, Brookfield VT, USA, 1992) 229.
13. P. DURAN, J. TARTAJ, J. F. FERNANDEZ and C. MOURE, *Ferroelectrics* **128** (1992) 231.
14. J. COLLIER, I. A. CORNEJO and M. J. HAUN, *ibid.* **154** (1994) 57.
15. Y. D. KIM, S. M. LANDIN, I. A. CORNEJO and M. J. HAUN, in "Proceedings of the IEEE International Symposium on Application on Ferroelectrics 1994", edited by R. K. Pandey, S. T. Liu and A. Safari (IEEE Inc., Piscataway, NJ, 1995) in press.
16. M. H. SLAYTON and H. S. N. SETTY, in "Proceedings of the IEEE International Symposium on Application on Ferroelectrics 1990", edited by S. B. Krupanidhi and S. K. Kurtz (IEEE Inc., Piscataway, NJ, 1991) pp. 90–2.

Received 6 February
and accepted 22 March 1995